Polyethylene-silver-zeolite composite coatings on stainless steel; corrosion resistance and antimicrobial characteristics

Materials Today Communications 49 (2025) 113874

Contents lists available at ScienceDirect

Materials Today Communications

journal homepage: www.elsevier.com/locate/mtcomm

Polyethylene-silver-zeolite composite coatings on stainless steel; corrosion resistance and antimicrobial characteristics

Soudabeh Shirani [a], Rahmatollah Emadi [a,*], Abdolmajid Eslami [a], Abdollah Saboori [b,c,**]

[a] Department of Materials Engineering, Isfahan University of Technology, Isfahan 84156-83111, Iran
[b] Department of Management and Production Engineering (DIGEP), Politecnico di Torino, Torino 10129, Italy
[c] Integrated Additive Manufacturing Center (IAM@PoliTo), Politecnico di Torino, 10129, Italy

ARTICLE INFO

Keywords:
Coating
Composite
Polyethylene
Zeolite
Silver
Stainless Steel
Antimicrobial

ABSTRACT

Due to various microbial species and decreasing healthcare costs, antimicrobial materials have become indispensable for human society. Silver ions are among the most widely used and effective antimicrobial agents, capable of penetrating bacterial structures and disrupting their biological systems. In this research, silver ions were first introduced to the porous zeolite network through an ion exchange mechanism. Then, high-density polyethylene (HDPE) coatings containing 0, 10, 20, and 30 wt.% silver zeolite were used to coat AISI 304 stainless steel using immersion methods. Subsequently, X-ray diffraction (XRD), scanning electron microscopy (SEM), Fourier-transform infrared spectroscopy (FTIR), adhesion tests, contact angle measurements, and roughness analysis were employed for the characterization of the coatings. The results indicated that increasing the silver zeolite content in the polyethylene matrix resulted in a more uniform coating with increased thickness and corrosion resistance while decreasing its adhesive strength. Furthermore, the corrosion resistance of the coatings using a 5 % sodium chloride salt spray for 800 h confirmed their good corrosion resistance. Finally. The antimicrobial performance of the samples was evaluated against *Escherichia coli*, *Staphylococcus aureus*, *Pseudomonas aeruginosa*, and *Aspergillus flavus* using MIC, MBC, MFC, zone of inhibition, and colony count assays. Results demonstrated that increasing silver zeolite content significantly enhanced antimicrobial efficacy, with the strongest activity observed against *Staphylococcus aureus*. These findings highlight the broad-spectrum antimicrobial potential of silver-zeolite composite coatings.

1. Introduction

Due to the rising threats posed by microbial pathogens and the increasing demand to reduce healthcare costs, materials with inherent antimicrobial properties have become essential for human applications. In recent years, significant research has focused on developing materials that possess intrinsic antimicrobial activity to prevent infections and enhance public health. Compared to conventional chemical antibacterial agents, which require frequent reapplication due to diminished efficacy, materials with inherent antimicrobial properties maintain long-lasting activity[1,2]. Such durable antimicrobial behavior makes these materials highly advantageous for a wide range of applications, including medical devices, coatings, and packaging, textiles, cosmetics, agriculture, and the environment where sustained microbial inhibition is critical[3].

Antimicrobial coatings have gained significant attention due to their critical role in controlling microbial growth across a wide range of industries, including textiles, medical devices, food packaging, water purification, paints, air and water filtration systems, agriculture, and energy sectors[4]. These coatings not only prevent surface contamination but also contribute to reducing healthcare costs and limiting the spread of infectious diseases[5]. Among the most effective antimicrobial agents for industrial applications are chitosan, carbon nanotubes, peptides, plant extracts, silver (Ag), copper, zinc, and transition metal oxides such as titanium dioxide, copper oxide, and zinc oxide[6]. Silver, in particular, has emerged as a highly potent antimicrobial agent owing to its unique physicochemical properties and broad-spectrum activity. Its antimicrobial effect primarily arises from the Ag^+ cation, which can penetrate microbial cells and interact strongly with electron-donating functional groups, including sulfur, oxygen, and nitrogen, present in

* Corresponding author.
** Corresponding author at: Department of Management and Production Engineering (DIGEP), Politecnico di Torino, Torino 10129, Italy.
E-mail addresses: remadi@iut.ac.ir (R. Emadi), abdollah.saboori@polito.it (A. Saboori).

https://doi.org/10.1016/j.mtcomm.2025.113874
Received 27 June 2025; Received in revised form 17 September 2025; Accepted 19 September 2025
Available online 20 September 2025

biomolecules [7]. These interactions disrupt enzymatic activity, protein function, and metabolic pathways, while binding to bacterial DNA and RNA, thereby inhibiting replication and transcription. Silver further offers advantages such as high thermal stability, low cytotoxicity, and long-lasting antimicrobial performance, which make it particularly suitable for diverse industrial and biomedical applications. Recent research has focused on integrating silver into coatings and composite materials in a controlled manner to enable sustained ion release, enhancing antimicrobial efficacy over extended periods [8]. The development of such durable antimicrobial coatings is crucial for applications requiring continuous microbial control, including medical implants, surface coatings, and packaging materials[9]. By combining silver with polymeric, inorganic, or hybrid matrices, it is possible to achieve multifunctional materials that exhibit mechanical robustness, chemical resistance, and prolonged antimicrobial activity[10]. This combination of properties not only improves the safety and durability of products but also supports environmental sustainability by reducing the frequency of chemical disinfectants [11]. Zeolites are a group of hydrated crystalline aluminosilicates with fine porosity, containing exchangeable cations from alkali and alkaline earth metal groups (Na^+, K^+, Mg^{2+}, and Ca^{2+}). They reversibly adsorb and release water [12]. The basic units of zeolites consist of tetrahedra SiO_4 and AlO_4 structures interconnected by oxygen atoms[13]. Secondary building units include rings and simple structures, and each zeolite comprises one or more types of these units[14]. During the ion exchange process, Na^+ ions are replaced by Ag^+ ions, giving the resulting zeolite new properties, such as antibacterial characteristics[15,16]. The environmental conditions suitable for releasing metal ions on the surface are precisely the conditions conducive to the survival or growth of biological pathogens on the surface[17]. The rate of silver release in zeolites is controlled, meaning that silver is only released when substituted with another ion. Additionally, silver is released from zeolites only in the presence of moisture [18]. While using zeolites in the structure of antimicrobial materials may reduce mechanical properties[19], it remains a suitable solution as a base for incorporating silver into materials with antibacterial and corrosion-resistant properties[20].

It is well documented that polymer coatings provide excellent corrosion resistance for cement and steel structures due to their high chemical resistance, suitable adhesion, and good mechanical properties. In these coatings, corrosion resistance is achieved through physical barriers and absorbents for corrosive agents [21]. Additionally, by shifting the corrosion potential towards more noble values, the corrosion rate of the metal surface decreases [22]. Considering the behavior of polymer coatings, promising properties can be achieved using additives to synthesize organic and inorganic composite materials. Additives can be zero-dimensional (including nanotubes and fibers), one-dimensional (including mineral materials like zeolites), and two-dimensional (including spherical particles) [23].

Due to the extensive use of steel, various protective methods have been considered to enhance its corrosion resistance, with organic coatings as the most common solution. Among them, polyethylene coatings, especially high-density polyethylene, are widely used due to their resistance to corrosive and chemical environments [24]. This polymer exhibits excellent resistance to penetration by water molecules and corrosive agents. Some advantages of polyethylene coatings compared to chemical inhibitors include their easy application, non-toxic nature, and minimal environmental and human health impact[25]. However, undesired problems associated with the incorporation of hydrophilic or polar organic and inorganic compounds into the above polymers including aggregation and weak distribution, as a consequence of immiscibility and incompatibility, and inability to recycle these materials have limited their processing conditions and product features [26]. In recent years, extensive studies have been conducted on using polymer coatings on metals and alloys to prevent corrosion. Composite coatings with a polymer matrix not only have good mechanical properties but also benefit from the presence of natural clinoptilolite zeolite particles ion-exchanged with silver, providing excellent antimicrobial, membrane, abrasion, and corrosion protection properties[3,27]. Despite all these advantages, the most important of which are the low cost and practicality of the coating, there is a gap in the literature on steel coating via polyethylene-zeolite-silver. Hence, In this study, the synthesis and characterization of silver-exchanged zeolite powder prepared from natural clinoptilolite, along with the fabrication of high-density polyethylene composite coatings containing silver zeolite via the dip-coating method, are presented. The properties targeted for evaluation include physical characteristics such as surface morphology by scanning electron microscopy (SEM), crystalline structure by X-ray diffraction (XRD), chemical bonding by Fourier-transform infrared spectroscopy (FTIR), and coating hydrophobicity as well as mechanical performance, assessed through adhesion testing. In addition, the integrity of the coatings under salt-spray conditions and microbiological assays for antibacterial efficacy were conducted to identify the most effective composite formulation as an antimicrobial agent.

2. Experimental

2.1. Materials

A natural celinoptilolite zeolite was used as feedstock material in this research. It should be noted that celinoptilolite ($Na_{3.12}\ Ca_{1.32}\ K_{0.72}\ Al_{8.11}\ Si_{27.84}\ O_{87.92}$) with a particle size in the range of 2– 5 mm can be found in nature. Commercial high-density polyethylene powder ($(-CH_2-CH_2-)_n$ linear) was used as a base polymer to prepare the coating. For Dip coating, Xyelene ($C_6H_4(CH_3)_2$ (Merk, Germany) was used for HDPE solubilization. The Silver ions were obtained using 99 wt.% Silver nitrate $AgNO_3$ (Merk, Germany).

2.2. Specimen preparation

Table 1 shows the chemical composition of the 304 stainless steel samples with a dimension of $20 \times 2 \times 2\ mm^3$ used as the metal substrate. To clean the surfaces, all substrates were ground with #80, #180, and #320 grit sandpaper, then degreased in acetone and dried at room temperature. The samples were then immersed in a solution of acids containing sulfuric acid, hydrochloric acid, and double distilled water with a volume ratio of 1:1:8 mL for 1 min to eliminate the oxide layers and activate the surface before being washed and air dried.

2.3. Silver incorporation in clinoptilolite zeolite

Natural clinoptilolite zeolite containing sodium and calcium with a chemical formula of ($Na_{3.12}\ Ca_{1.32}\ K_{0.72}\ Al_{8.11}\ Si_{27.84}\ O_{87.92}$) was milled using a ball mill with steel balls at a ball: powder weight ratio of 10:1 at a speed of 200 rpm for 3 h to reduce the particle size. After milling, the powder was sonicated for 20 min in an ultrasonic bath and then washed for 60 min with 70% ethanol using a magnetic stirrer at 300 rpm. The resulting material was filtered through filter paper and then dried in an oven at 80 ℃. The obtained powder was further washed for 60 min with a hydrochloric acid solution and water with a 10:90 vol ratio on a magnetic stirrer and subsequently filtered through filter paper and dried at 60 ℃. It is worth noting that the acid treatment of natural clinoptilolite zeolite removes impurities such as calcium carbonate and increases the specific surface area of the zeolite. A quantity of 3 g of zeolite powder was mixed with 1 g of silver nitrate powder in 200 mm of water and subjected to distillation for 16 h at 60 ℃ on a magnetic stirrer to facilitate ion exchange between the silver nitrate particles and the zeolite. During this process, the container was covered with aluminum foil to prevent direct exposure to light since light exposure can cause oxidation and darkening of the silver nitrate particles. After the desired time for ion exchange of the silver nitrate particles with the zeolite was completed, the solution was filtered through filter paper, which had fine pores for separating the silver zeolite powder from the aqueous phase.

Table 1
The chemical composition of the 304 stainless steel substrate.

Fe	C	Si	Mn	Cr	Mo	Ni	Al	Co	Cu	V	W	Sb
Bal.	0.0649	0.412	1.56	19.0	0.0953	8.88	0.0024	0.126	0.190	0.0667	0.0156	0.0289

2.4. Preparation of composite coating

To prepare a coating suspension, silver zeolite particles were dispersed in 20 mL of xylene for 20 min in an ultrasonic bath. Subsequently, polyethylene powder (HDPE) was added to the suspension. To enhance polymer adsorption on the surface of the prepared suspension particles, the mixture was subjected to mechanical agitation for 7 h at a speed of 200 rpm. Suspensions with varying weight percentages of silver zeolite, specifically 10, 20, and 30 wt./wt.%, were then formulated for coating. The prepared suspension was dissolved in xylene at a temperature of 90 ºC. Steel samples were prepared and submerged in the solution three times using a dip-coating apparatus, with each immersion conducted at a speed of 2 mm/s. After each 2-minute immersion, the samples were taken from the solution at the same speed. Following the completion of the coating process, the samples were dried at 60 ℃ for 24 h. Fig. 1. shows a schematic of the silver zeolite polyethylene composite coating on 304 stainless steel by dip coating method. The samples are identified with the following codes in Table 2.

Table 2
Coding of samples coated with silver zeolite polyethylene composite.

sample code	type	Composition
P100	The pure polyethylene coating	0.5 g PE
P−10ZA	The polyethylene composite coating - 10 % silver zeolite	0.45 g PE + 0.05 g ZA
P−20ZA	The polyethylene composite coating - 20 % silver zeolite	0.4 g PE + 0.1 g ZA
P−30ZA	The polyethylene composite coating - 30 % silver zeolite	0.35 g PE + 0.15 g ZA

2.5. Characterization

The characterization of silver-exchanged zeolite was carried out using X-ray diffraction spectroscopy (XRD, ASENWARE, AW-XDM300, china), scanning electron microscopy (SEM, Philips, XL 30, Netherlands) equipped with EDS analysis and Fourier transform infrared Spectrometer in the range of 400–4000 cm^{-1}. (FTIR, Bruker, Tensor 27, German). The present study investigated the impact of various weight percentages of silver zeolite on the hydrophilicity of pure HDPE and HDPE-silver zeolite. The contact angle of various samples with water was assessed following the ASTM D5964 standard for analysis.

Surface wettability assessment of the samples was conducted using the KVS, 500A-CA equipment. Subsequently, the surface roughness was evaluated. The evaluation of adhesion strength between the coatings and the substrate followed the ASTM D3359 standard, employing the crosshatch tape method. This procedure introduced six deep cuts on the samples in both directions, with a minimum distance of 1 mm between each cut. Subsequently, the adhesion test was conducted by applying and detaching the tape from the coating surface at the points of intersection of the cuts. Adhesion was quantified based on the number of squares removed from the surface, utilizing a 0–5B scale. A rating of 5B denoted the optimal adhesion (no square or edge damage), while 0B indicated the weakest bonding strength (all squares were damaged or removed from the surface). Salt spray experiments were carried out to assess the visual performance of the samples. In this experiment, coatings with x-scratches were subjected to the salt spray test using the S83 V4300 salt spray test cabin (manufactured by Pars Horm Co.) following ASTM B117 standards (NaCl 5 wt. % solution) for 800 h.

2.6. Antibacterial testing

The antibacterial efficacy of the polyethylene-silver zeolite composite was assessed against *Staphylococcus aureus* ATCC6538 (gram-positive bacteria) and *Escherichia coli.* ATCC10536 (gram-negative bacteria) strains. The agar well diffusion method was employed to determine the antibacterial activity of the selected extracts. Nutrient agar was prepared, autoclaved, and allowed to solidify at room temperature. Autoclaved agar plates were inoculated with bacterial cell suspensions. Wells (5 mm) were created in each agar plate using a sterile metallic borer. Each well was loaded with 80 μL (1 mg/mL) of the sample with *E. coli.* and S. aureus, serving as negative and positive controls, respectively. All plates were then incubated at 37 °C for 24 h, and the results were quantified by measuring the zone of inhibition in millimeters. Bacterial cell counting or colony counting is one of the various biological processes where the number of bacterial cells is quantified in a specific volume. By placing a defined volume of cultured cells on a Petri dish containing a culture medium, the number of cultured cells can be enumerated. If cells are appropriately distributed in the culture medium, it can be assumed that each cell creates a single colony. Therefore, colonies are countable, and based on the specified volume of the distributed culture medium in the dish, the cell concentration can be calculated. Performing bacterial colony counting is useful for estimating the infectivity of bacterial infections, such as beneficial

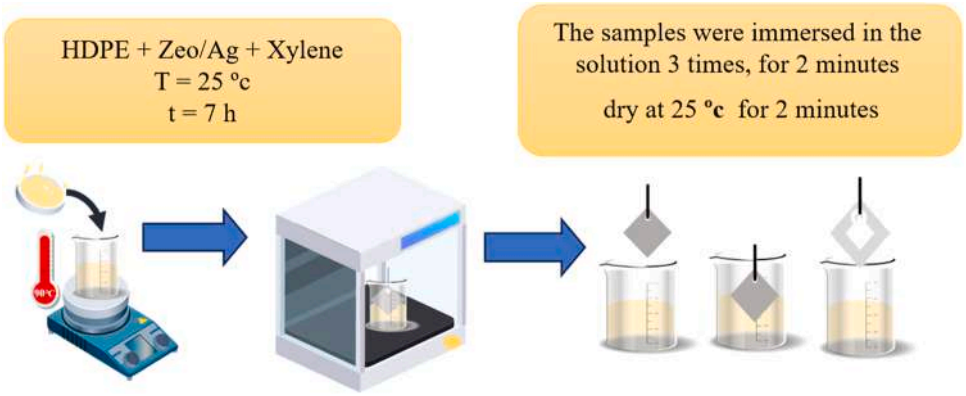

Fig. 1. Schematically illustrates the composite coating of silver zeolite-polyethylene on 304 stainless steel by the dip-coating method.

bacterial infections. *S. aureus* (ATCC 6538) as a Gram-positive bacterium and *E.coli*. (ATCC 10536) A Gram-negative bacterium was prepared at a specific concentration in a normal saline solution according to the 0.5 McFarland concentration. Then, 30 % samples were incubated for 24 h at a temperature of 37 ± 2 °C.

The culture medium, along with the bacterial suspension, was considered as a positive control for both bacterial strains. After this period, serial dilutions of each sample were performed, and 10^{-6} and 10^{-1} dilutions of bacterial-containing samples were prepared. A specified amount of the 10^{-6} dilution was streaked on an agar culture medium, spread on the surface, and incubated for 24 h at 37 ± 2 °C. The number of colonies in each mentioned concentration was then counted, and the increase or decrease in the colony count was assessed relative to the control sample. This description outlines a microbiological experimental procedure for assessing bacterial colony formation to measure infectivity.

2.7. Determination of minimum inhibitory and bactericidal/fungicidal concentrations (MIC, MBC, MFC)

The antimicrobial efficacy of the tested samples was evaluated against four representative microorganisms: Escherichia coli (Gram-negative), Staphylococcus aureus ATCC6538 (Gram-positive), Pseudomonas aeruginosa, and the fungal strain Aspergillus flavus ATCC 22548.

MIC determination was performed using a standard broth microdilution method. Briefly, microbial suspensions were prepared in suitable liquid culture media and adjusted to a concentration corresponding to 0.01 % of a McFarland standard. Serial dilutions of each test sample were prepared in the liquid medium, and aliquots were inoculated with a defined volume of microbial suspension. Negative controls (culture medium without microorganisms) and positive controls (culture medium with microorganisms but without the sample) were included in each assay. All test tubes were incubated at 37 ± 2°C for 24 h for bacterial strains, while fungal cultures were incubated under appropriate

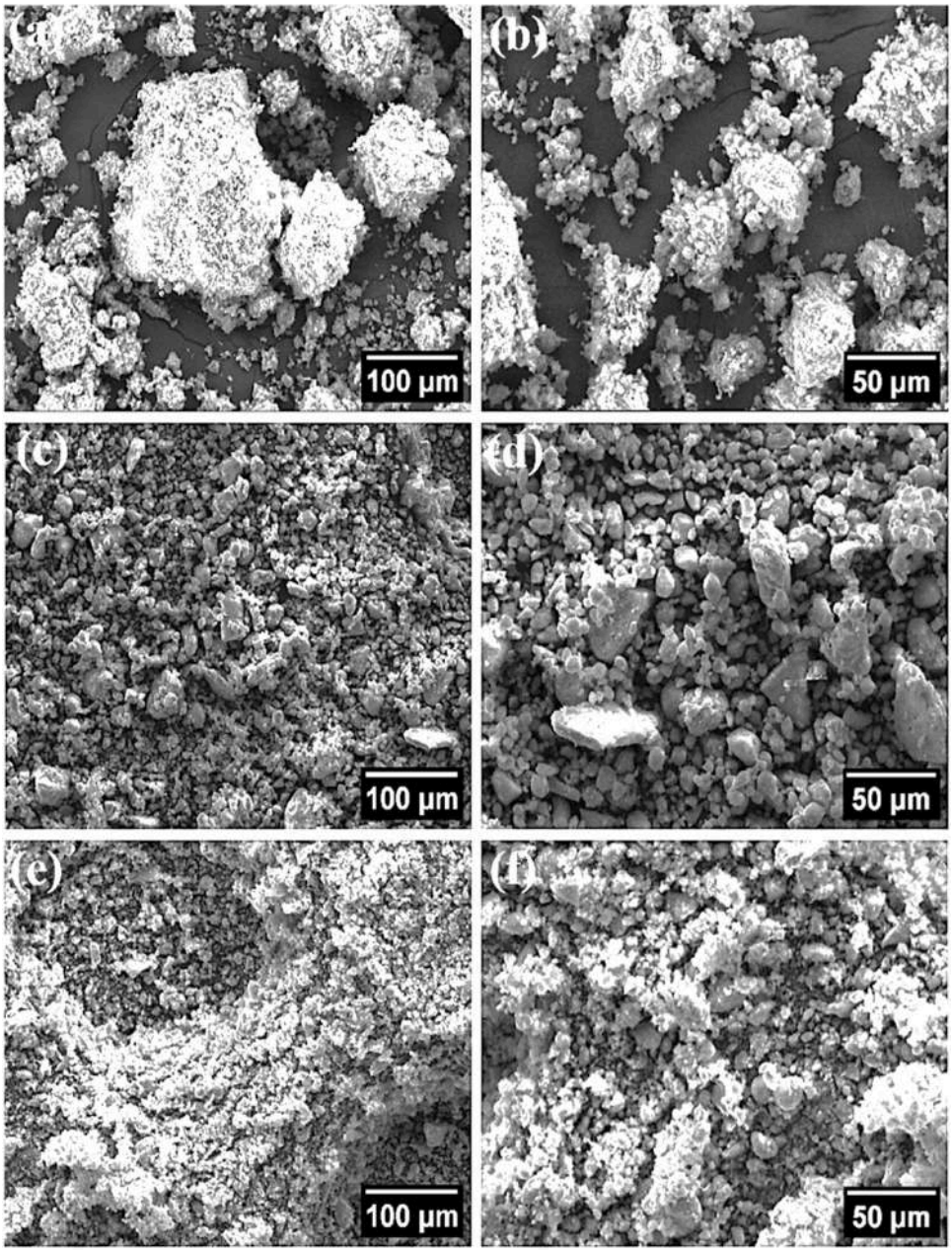

Fig. 2. SEM images (a, b) zeolite powder washed with ethanol (c, d) zeolite powder washed with HCl (e, f) ion-exchanged zeolite powder using $AgNO_3$.

conditions. After incubation, turbidity was assessed visually to determine the minimum inhibitory concentration (MIC), defined as the lowest concentration of the sample that prevented visible microbial growth.

To determine the minimum bactericidal/fungicidal concentration (MBC/MFC), aliquots from the MIC tubes were transferred onto solid agar plates and incubated under the same conditions. The lowest concentration at which no colony formation was observed on agar was recorded as the MBC for bacteria and MFC for the fungal strain. This step allows differentiation between inhibitory and lethal effects of the tested material.

All assays were performed in triplicate to ensure reproducibility, and results were expressed as mean ± standard deviation. This comprehensive approach enables precise evaluation of the antimicrobial potential of the samples across both bacterial and fungal models, providing insights into their broad-spectrum efficacy.

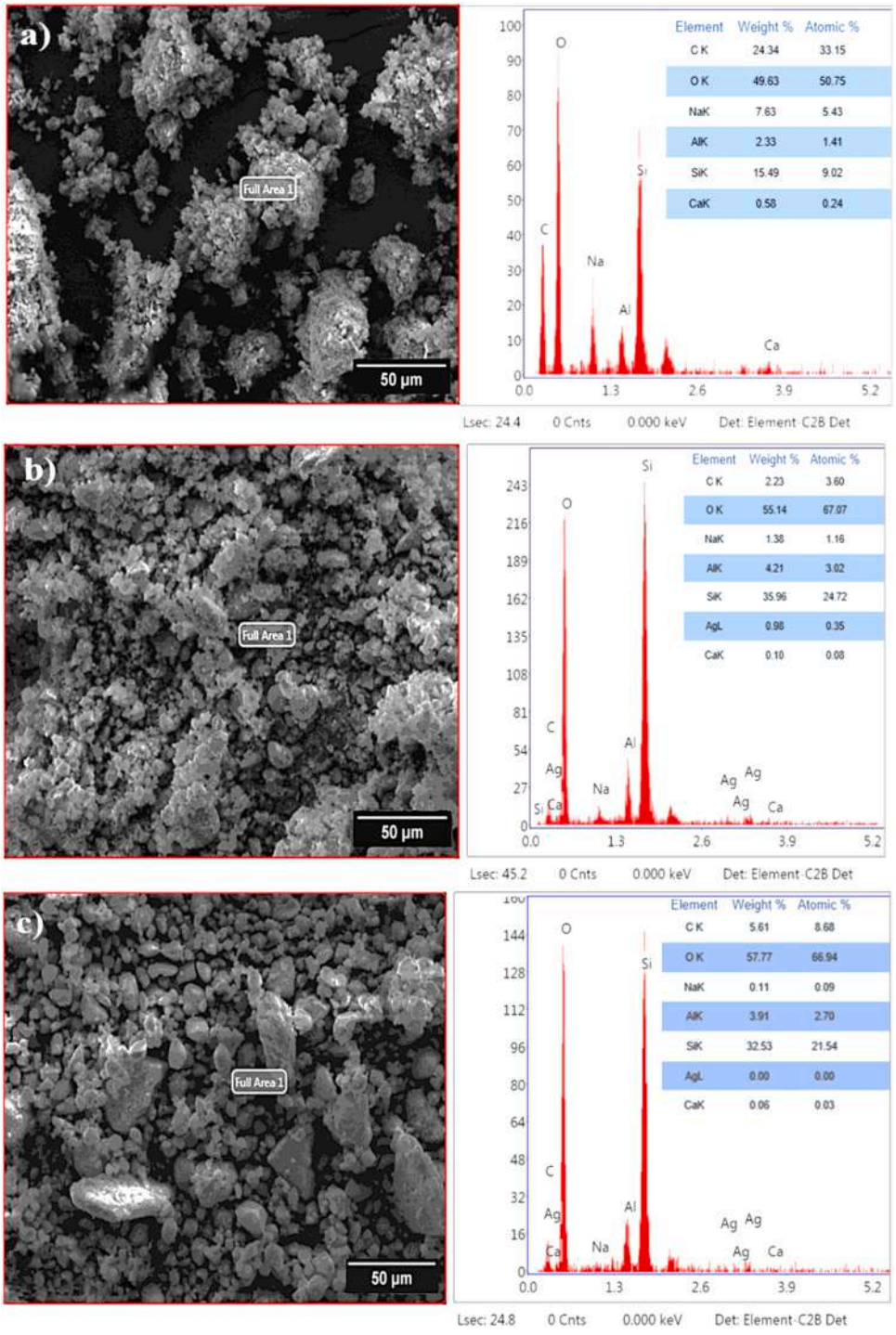

Fig. 3. Elemental analysis obtained by scanning electron microscopy (a) zeolite powder washed with ethanol, (b) zeolite powder washed with HCl, (c) ion-exchanged zeolite powder using $AgNO_3$.

3. Results and discussion

3.1. Microstructure and composition

The SEM images shown in Fig. 2. illustrate a washed natural clinoptilolite zeolite powder sample treated with ethanol. Due to the presence of impurities and the inherent nature of the zeolite powder, the particles appear clustered. Upon washing with hydrochloric acid, various phases present in the powder, including calcium carbonate and sodium carbonate, are removed, reducing the impurities in the powder. After the ion exchange stage with silver nitrate, silver ions replace calcium and sodium ions in the porous structure of the powder. The acid treatment of the zeolite powder results in a significantly increased specific surface area due to the removal of calcium carbonate formed on its surface.

Additionally, the SEM images of the zeolite powder containing silver indicate no noticeable change in the powder morphology, and silver particles are uniformly distributed within the zeolite structure [28,29]. Furthermore, the average particle size of the natural zeolite after milling and ion exchange is approximately 11.5 ± 3.24 μm. These observations suggest that the processing steps, including acid treatment and ion exchange, have specific effects on the composition and morphology of the zeolite powder, particularly enhancing its surface characteristics and incorporating silver ions into its structure.

The EDS pattern of zeolite was prepared both in its initial form and after ion exchange, as shown in Fig. 3. As observed, the main peaks corresponding to the elements Al, Si, and O in the EDS spectrum represent the major elements of zeolite. Additionally, peaks related to the elements Na and Ca are identified, indicating the presence of natural clinoptilolite zeolite. Aluminum and silicon form tetrahedral bonds with oxygen and sodium ions within the zeolite framework and stabilize the negative charges of aluminum on the zeolite surface. Upon the introduction of silver into the zeolite, a reduction in the peaks related to Na and Ca and the appearance of the Ag peak are observed [16,30,31]. This phenomenon can result from the ion exchange, where the Na and Ca ions concentration in the zeolite powder is reduced. Conversely, the concentration of Ag ions is increased. Moreover, the intensity of the added Ag peak is higher than the intensity of the reduced Ca peak. This suggests that not all the displayed Ag in the figure is exchanged with Ca and Na; a small amount may have formed deposits such as AgOH and AgCl.

3.2. XRD powder analysis

The XRD analysis results for the washed clinoptilolite powder with ethanol, hydrochloric acid, and silver-ion exchanged are presented in Fig. 4. Considering the X-ray diffraction pattern of Zeo-Ethanol and the presence of main peaks at 2θ = 8.9, 11.2, 22.4, 27.2, 26.1, 28.2, 30, 32, and 36.4° angles, the existence of clinoptilolite zeolite is confirmed, consistent with the JCPDS [96–900–1395] database. The peaks are initially tall and sharp, becoming shorter and broader in the Zeo-HCl pattern due to acid treatment with hydrochloric acid, indicating the disruption of its crystalline structure. The Zeo-Ag pattern shows no significant changes in the zeolite structure or phase alteration for the ion exchange process. However, there is a clear reduction in the intensity of the peaks in the Zeo-Ag pattern for the zeolite. This pattern is attributed to the incorporating of silver and other cations into the zeolite structure, leading to a redistribution of internal cationic charges and a loss of the crystalline structure[31]. Additionally, the study by R. Garza et al. found that the ion exchange of clinoptilolite zeolite with silver did not result in significant changes in the XRD pattern [32]. In another study by Xu et al., the addition of 73.365 mg/g of silver to zeolite type A showed no observable structural changes in the X-ray diffraction pattern, indicating an efficient cation exchange process [31]. In this research, the presence of active chlorine ions resulting from acid washing led to the formation of AgCl phases with the JCPDS [96–901–1667] code. The image shows samples of coated P100, P-10ZA, P-20ZA, and P-30ZA with various

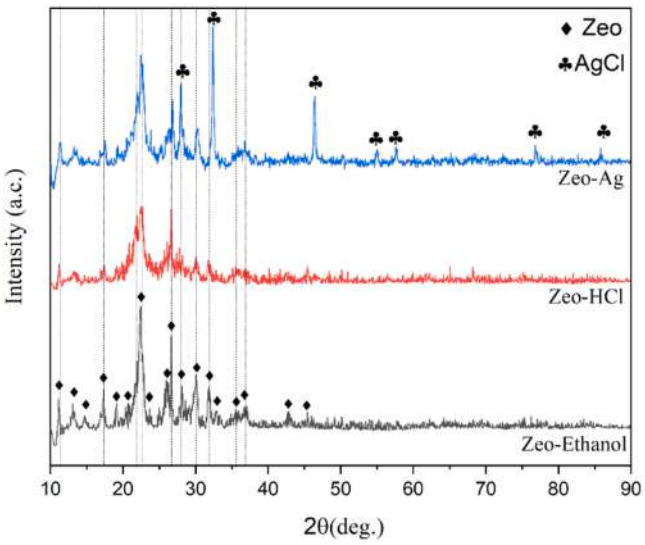

Fig. 4. XRD pattern of (a) Zeo-Ethanol (zeolite powder washed with ethanol), (b) Zeo-HCl (zeolite powder washed with hydrochloric acid), (c) Zeo-Ag (ion-exchanged zeolite powder using $AgNO_3$).

percentages of silver zeolite at three different magnifications. With an increase in the percentage of silver zeolite, a relatively good dispersion of silver zeolite on the polymer surface can be observed. The regular dispersion of silver zeolite on the polymer surface is of special importance due to its desired high efficiency. The increasing amount of silver zeolite enhances the specific antibacterial property efficiency. As mentioned earlier, the integration of silver into the zeolite does not alter its morphology and crystal sizes. Furthermore, silver zeolite does not induce any structural changes in the polymer.

3.3. SEM coating analysis

In Fig. 5. the coated samples P100, P-10ZA, P-20ZA, and P-30ZA with various percentages of silver zeolite are shown at two different magnifications. With an increase in the percentage of silver zeolite, a relatively good dispersion of silver zeolite on the polymer surface can be observed. The uniform dispersion of silver zeolite on the polymer surface is of special importance due to the desired high efficiency. Considering the increase in the amount of silver zeolite, the efficiency of the antibacterial property increases. As mentioned earlier, incorporating silver into zeolite does not alter the morphology and sizes of zeolite crystals. Additionally, silver zeolite does not induce changes in the polymer structure.

In Fig. 6. the elemental analysis of the P100 sample shows that the coating is entirely carbon-based. In the subsequent samples, P-10ZA, P-20ZA, and P-30ZA, with an increase in the amount of silver zeolite, the amount of Ag increases, in addition to the base elements of zeolite Si and Al, while the carbon content of the coating is reduced. In the P-30ZA sample, the lowest amount of carbon and the highest amount of silver are observed.

The EDS elemental analysis maps of the P-10ZA, P-20ZA, and P-30ZA coatings are shown in Fig. 7. It can be observed that with an increase in the elements present in the composite coating, the elements are uniformly distributed on the surface.

Fig. 8. presents the elemental analysis mapping of the P-30ZA coating, selected as a representative sample to demonstrate the presence of silver zeolite elements on the cross-sectional surface of the coating. The uniform distribution of Si, Al, and Ag elements derived from natural clinoptilolite zeolite can be observed within the composite matrix.

In Fig. 9. the cross-sectional surface of the composite coatings can be observed, indicating a smooth and uniform surface on the 304 stainless

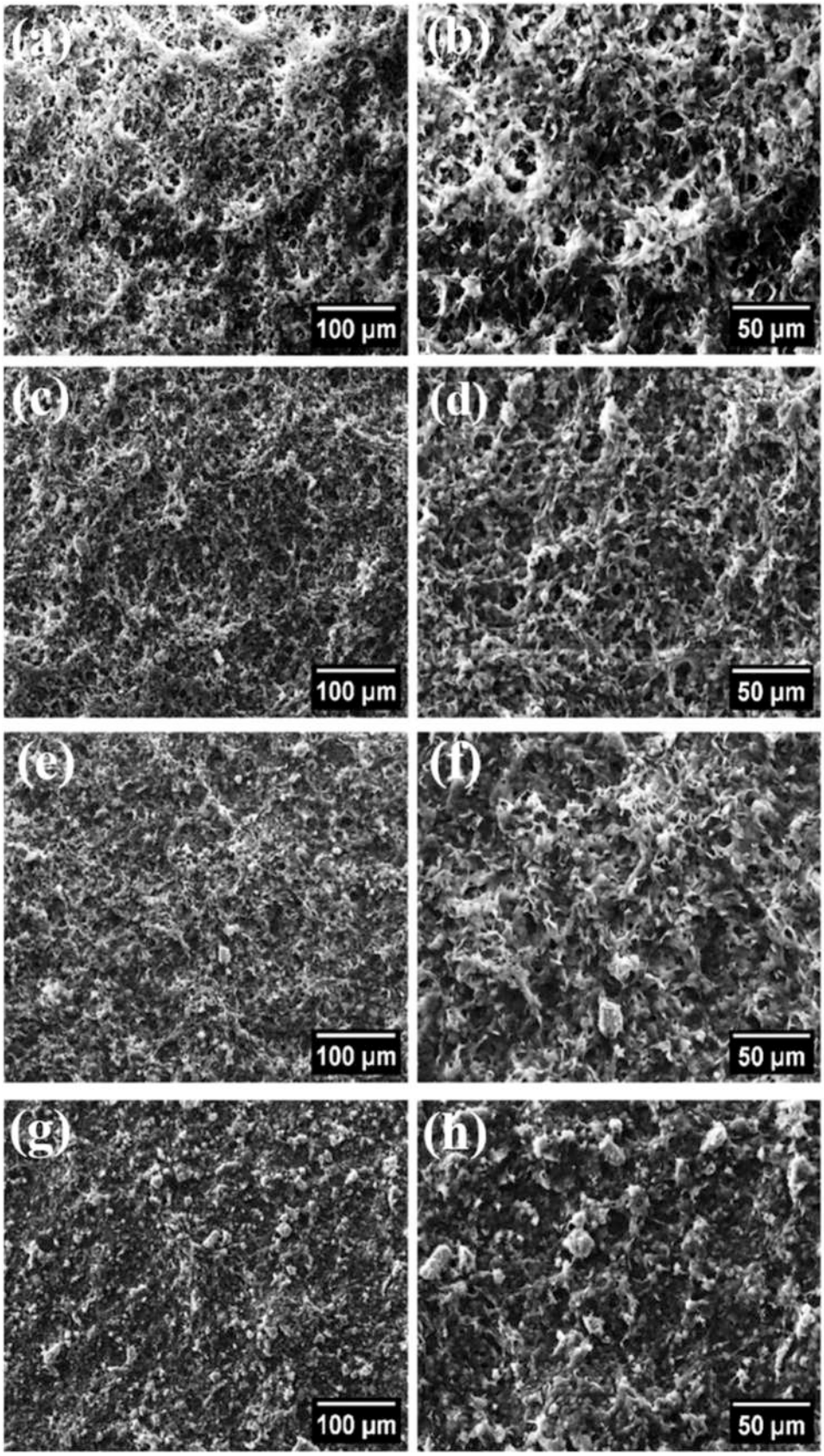

Fig. 5. SEM images of (a, b) P100 coating. (c, d) P-10ZA coating. (e, f) P-20ZA coating, and (g, h) P-30ZA coating.

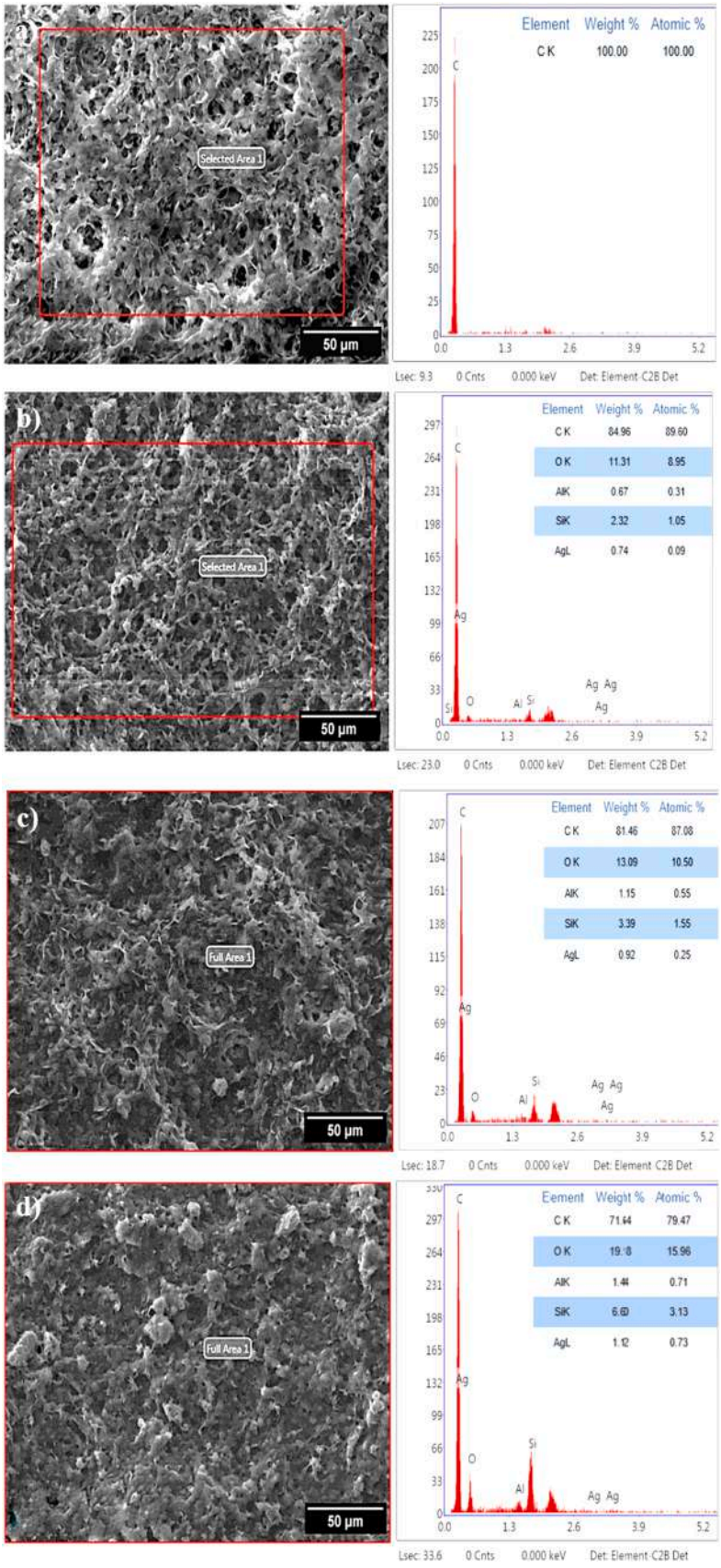

Fig. 6. Elemental analysis obtained by SEM-EDS for (a) P100, (b) P-10ZA, (c) P-20ZA, and (d) P-30ZA.

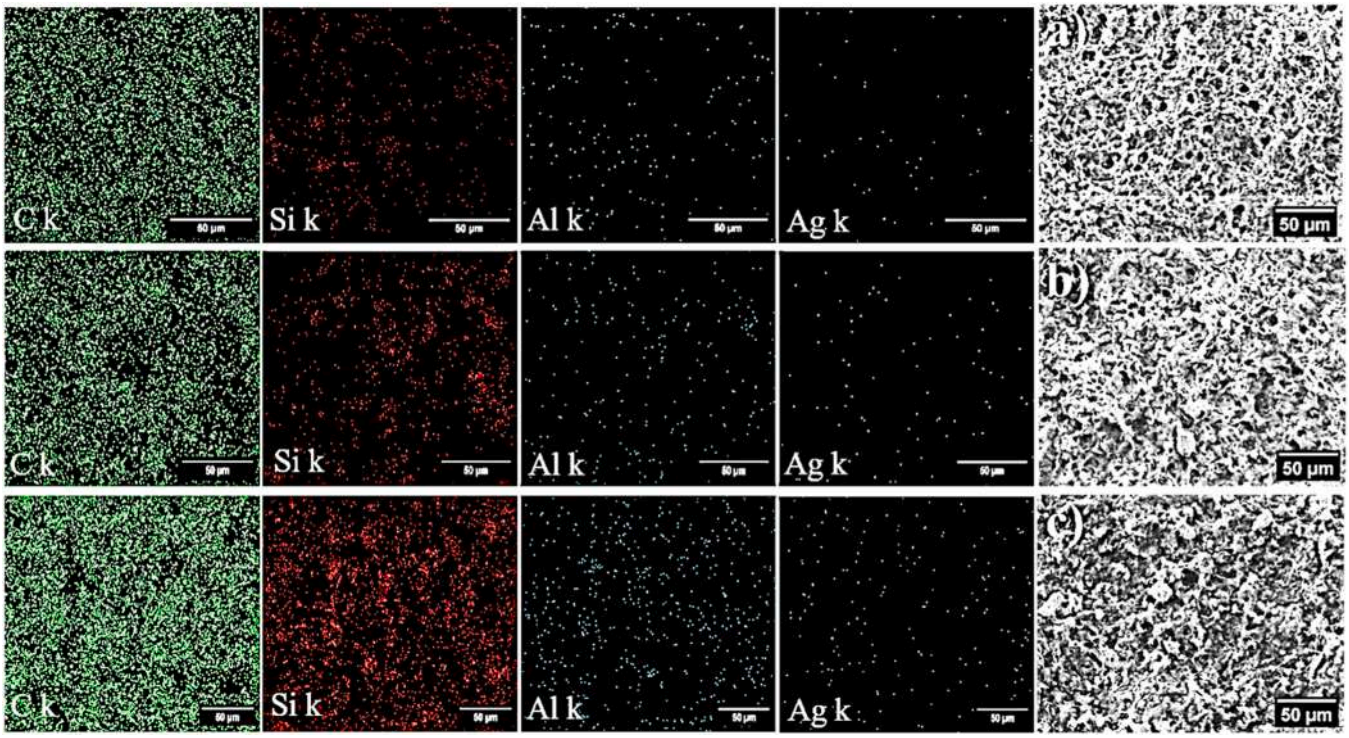

Fig. 7. Elemental mapping analysis of (a) P-10ZA, (b) P-20ZA, and (c) P-30ZA.

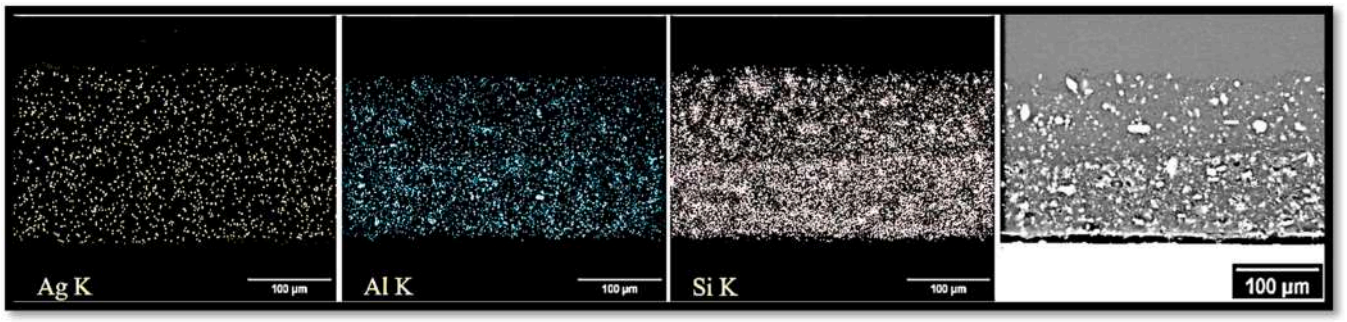

Fig. 8. EDS elemental mapping analysis of the cross-sectional surface of the P-30ZA coating.

steel without layering or cracking. The average thickness of the P100, P-10ZA, P-20ZA, and P-30ZA coatings is 98.1 ± 80.59, 99.4 ± 14.144, 100.4 ± 301.154, and 50.4 ± 174.168 µm, respectively. It can be noted that the thickness of the coating layers has increased with the addition of ceramic composite materials, and uniform distribution of silver zeolite can be observed in the coating layers, respectively. The increase in coating thickness may be attributed to the enhanced wetting effect of the coating. Furthermore, these results indicate that the immersion coating technique can deposit thick coatings, overcoming challenges associated with thick plasma-sprayed coatings (>100 µm)[28].

The porosity in the coating layers was estimated from microscopic surface images of the coatings using ImageJ software for selected samples P100, P-10ZA, P-20ZA, and P-30ZA, as shown in Fig. 10. The highest porosity is associated with the P100 coating, which is approximately equal to 22.3 %. The lowest porosity was calculated for the P-30ZA coating to be 10.2 %. Additionally, the porosity for the P-10ZA and P-20ZA samples are 19 % and 13.2 %, respectively. Considering that the percentage and size of porosity in the samples decrease with an increase in silver zeolite, it can be concluded that the porosity of the coatings is inversely proportional to the amount of ceramic composite materials. It can be inferred that silver zeolite particles have filled the voids in the polymeric matrix.

3.4. XRD coating analysis

The XRD patterns of the coatings for samples P100, P-10ZA, P-20ZA, and P-30ZA are illustrated in Fig. 11. The results indicate that two crystalline peaks at 21.5° and 23.9° with the JCPDS [00–050–2241] code, corresponding to the (110) and (200) planes, respectively, are related to polyethylene. The other observed peaks are attributed to silver zeolite and AgCl with the JCPDS [96–900–1395] and JCPDS [96–901–1667] code compounds. Both amorphous and crystalline sections of polyethylene are demonstrated, and no shift in the positions of polyethylene peaks is observed. This implies that various percentages of silver zeolite do not induce any changes in the polyethylene structure [33]. Additionally, it can be inferred that the intensity of polyethylene peaks decreases, and the peaks of zeolite and silver chloride increase with the rise in silver zeolite content.

3.5. FTIR analysis

The chemical composition of polyethylene and silver zeolite was

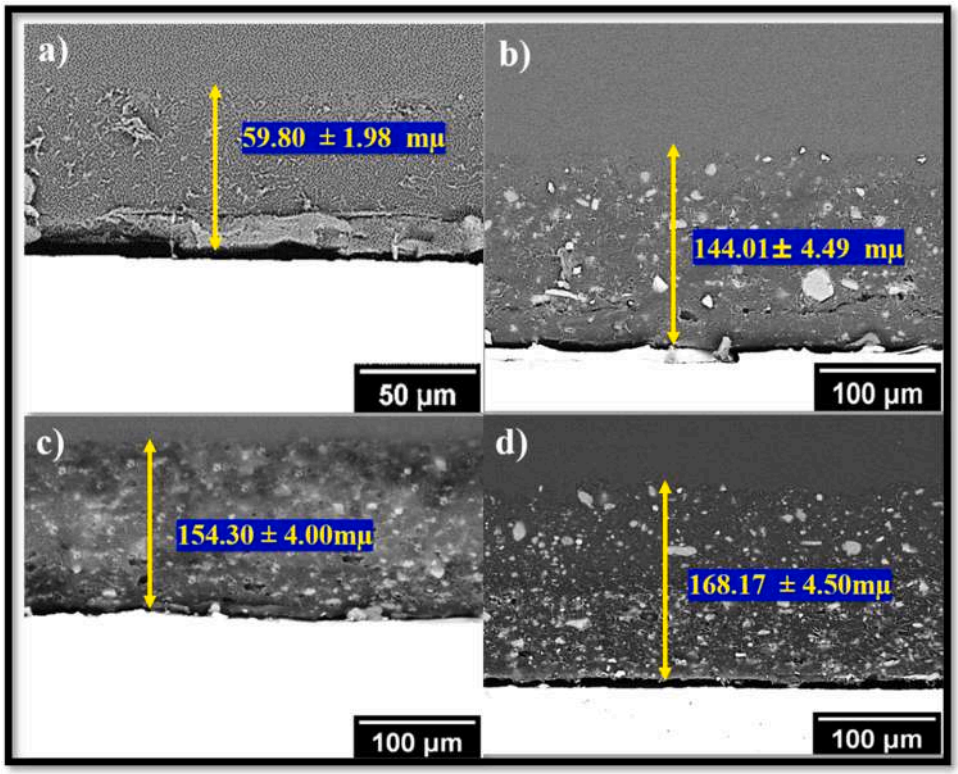

Fig. 9. SEM images of the cross-sectional surface (a) P100, (b) P-10ZA, (c) P-20ZA, (d) P-30ZA coating.

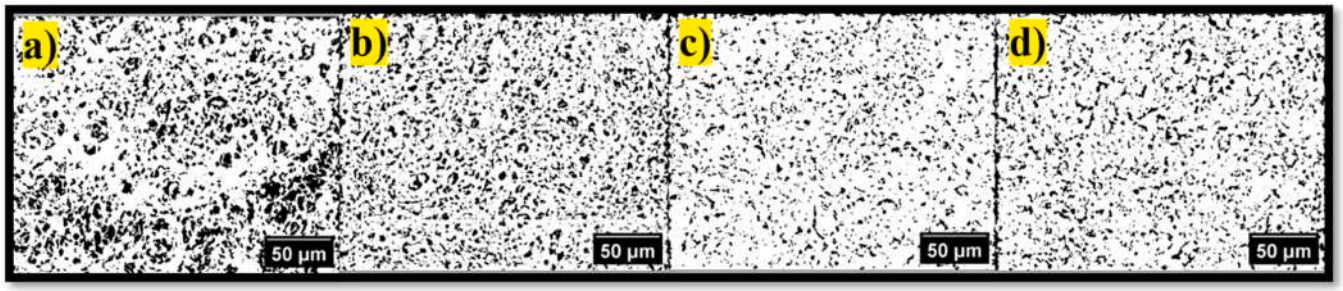

Fig. 10. Images of SEM (a) P100, (b) P-10ZA, (c) P-20ZA, (d) P-30ZA coating at a magnification of 50 microns after measuring the coating porosity using ImageJ.

investigated through Fourier-transform infrared (FTIR) spectroscopy analysis. Fig. 12. displays the obtained peaks from the FTIR test. The height of each peak serves as an indicator of the higher percentage of the corresponding bond. Moreover, a sharper peak suggests a more ordered structure of the substance. Table 3 illustrates the bonds present in the polymer coating at various wavenumbers.

Additionally, Table 4 corresponds to the peaks at different wavenumbers for the polyethylene coatings with silver zeolite.

3.6. Evaluation of the adhesion of the polyethylene silver zeolite composite coating

Fig. 13. illustrates the microstructure of the coated samples after the peel adhesion test. All four coating models have been classified into their respective classes. The coating of the P100 sample (3B), P-10ZA (4B), P-20ZA (5B), and P-30ZA (2B) are found in their appropriate classes. The adhesion is influenced by various factors such as coated layer thickness, surface roughness, percentage of added ceramic particles, and composite matrix (polyethylene). One of the adverse effects of adding an excessive amount of particles to the polymeric matrix is the creation of open and empty spaces at the particle-polymer interface due to the weak connection between polymer chains and silver zeolite particles[19]. This results in the formation of void spaces at the particle-polymer interface[30]. Additionally, an increase in the common phase between silver zeolite particles and the polyethylene matrix and the resulting internal stresses in the coatings containing these particles (beyond the optimal state) decrease the coating adhesion to the substrate. Therefore, the presence of silver zeolite particles in heavy polyethylene, at a weight percentage of 10 %, increases the relative adhesion of the coating to the substrate. With an increase in the silver zeolite content to 20 wt.%, the adhesion of the coating reaches its optimal state, represented by class (5B). However, with 30 wt.% of silver zeolite in the coating, we observe a reduced adhesion of the coating to the substrate. The reason for this mechanism is the result of voids between polymer-particle connections. Hence, the distribution of silver zeolite particles in heavy polyethylene leads to a relatively higher surface roughness and, consequently, a higher mechanical lock between polyethylene and particles. Coating thickness is another factor that must be considered [35]. As shown in Fig. 9. the thickness of the P100 coating is less than coatings with lower silver zeolite content, resulting in lower internal stresses and a reduced risk of coating detachment from the substrate. Since the thickness of P-30ZA is higher than that of other coatings but has lower adhesion

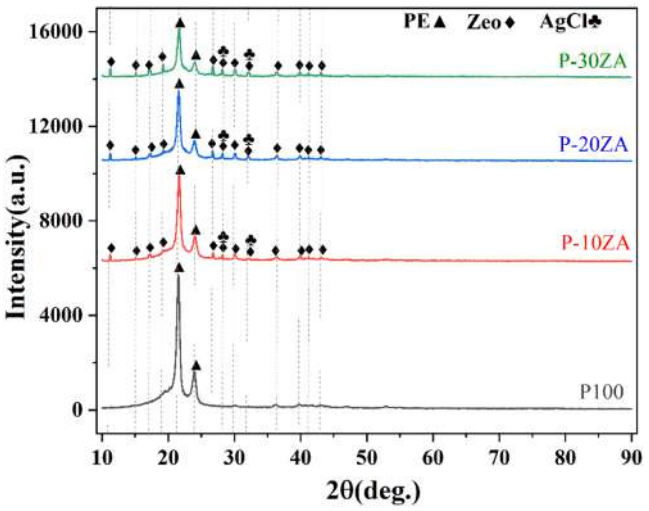

Fig. 11. XRD patterns of coated specimens: (a) P100, (b) P-10ZA, (c) P-20ZA, (d) P-30ZA.

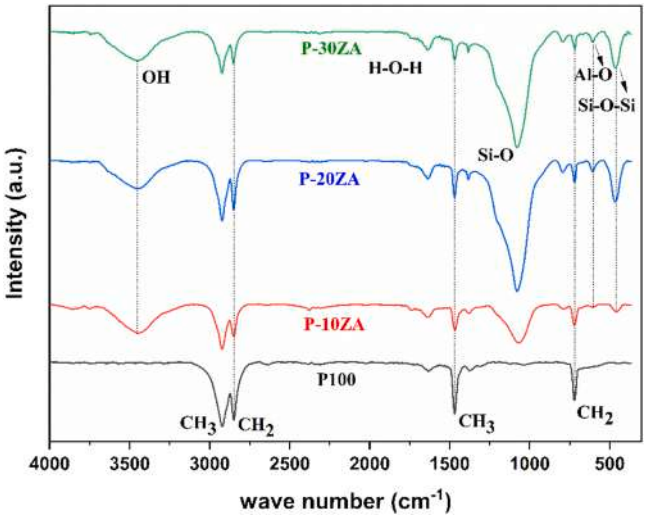

Fig. 12. FTIR spectra of coated specimens (a) P100, (b) P-10ZA, (c) P-20ZA, (d) P-30ZA.

Table 3
Bonding and wavenumber of polyethylene polymer [34].

Peak	Wavenumber [cm^{-1}]
CH_2 (Asymmetric)	2925
CH_2 (Symmetric)	2848
CH_2 (Wagging)	1467
CH_2)Rocking)	721

Table 4
Bonding and wavenumber of clinoptilolite zeolite particles [24].

Peak	Wavenumber [cm^{-1}]
OH	3450
H-O-H	1635
Si-O	1080
Al-O	605
Si-O-Si	464

compared to other coatings, it can be concluded that an increase in thickness of up to a relatively acceptable and suitable amount is preferable in the immersion coating model.

3.7. Wettability coating

Fig. 14. illustrates the wettability of the coated surfaces using water droplet contact angle measurements. After coating the substrate with heavy polyethylene (P100), the water repellency has a contact angle of 130.4°. Following the addition of silver zeolite up to 10 wt.%, consisting of crystalline hydrated aluminosilicates with fine porosity containing alkaline and alkaline earth metal cations, the contact angle decreases to 123°. In this state, the water droplet cannot wet the surface while maintaining its spherical shape (a, b). With an increase in the silver zeolite content to 20 and 30 wt. %, the contact angle decreases to 117 and 108.8°, respectively (Fig. 14c,d). Moreover, an increase in the content of silver zeolite particles in the coating forms a more uniform and dense coating. In this case, due to the high surface energy of the silver zeolite polyethylene coating, the cohesive forces of the water droplet are less than its adhesive forces to the surface. It is evident that most oxide ceramics are hydrophilic with an equilibrium contact angle close to zero. This can be attributed to the bonding energy of oxides with water molecules compared to water surface tension. Kho et al. attributed this phenomenon to the presence of many hydroxyl groups (OH^-) on the surface of SiO_2 particles [36].

3.8. Salt spray

Fig. 15. illustrates images from the salt spray test for samples P-10ZA (a, b), P-20ZA (c, d), and P-30ZA (e, f) before exposure to the salt spray apparatus and after 800 h of testing, respectively. Essentially, the polyethylene coating exhibits no discernible reaction with the sodium chloride environment, which can be attributed to its unique and regular $(CH2)_n$ structure. The results indicate that the adhesion loss of the coating after 800 h is negligible for the P-10ZA and P-20ZA samples, with the coating remaining attached to the substrate surface and no detachment observed during the wet adhesion test. Moreover, it can be noted that the coating withstands well beyond 800 h in the salt spray apparatus, signifying its robust protection in a moist environment. However, for the P-30ZA sample with scratches, adhesion is compromised after 800 h, and the coating fractures from the scratch site during the wet adhesion test. It is worth noting that water molecule penetration should be considered in a moist environment.

Studies suggest that water molecule penetration leads to swelling and reduced adhesion in polar polymer coatings. The less polar heavy polyethylene coating is highly impermeable to water and exhibits significant water repellency. Therefore, in the P-10ZA and P-20ZA samples, notable adhesion is not observed. Brewing notes that the effect of water penetration and softening is much more pronounced in polar polymers than in non-polar polymers; hence, wet adhesion is measured after a specific duration in humidity, termed "wet adhesion" [35]. Fank and Hagen observed that a film with water permeability and good wet adhesion provides effective protection. Fank argues that wet adhesion is the most critical parameter for a corrosion-resistant coating in a humid environment. Other factors, such as exposure duration, electrolyte presence in the joint season, permeation rate, reaction kinetics, corrosion products, and the presence of corrosion inhibitors, are crucial for initiating corrosion in a coating with weak adhesion. Bahl found that a weak adhesion itself is not the cause of poor corrosion resistance, and a surface coating can maintain its protective effect even with complete adhesion loss as long as it is a flawless, defect-free layer or if it possesses very good adhesion. However, both features together provide excellent corrosion resistance[37]. Bagheri investigated that polyethylene coatings containing stabilizers have better mechanical resistance and adhesion than simple polyethylene coatings after 700 h of salt spray testing. He also added that continuous exposure of a sample to salt spray

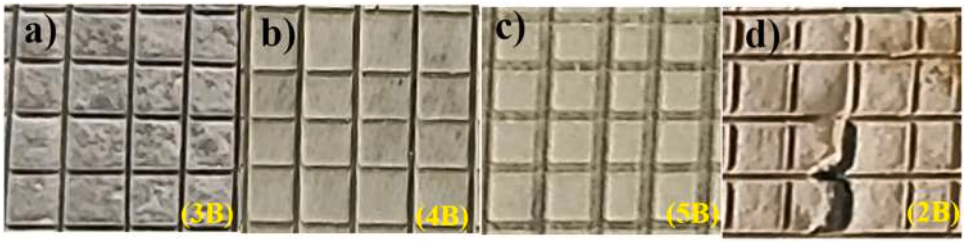

Fig. 13. Surface Image of (a) P100, (b) P-10ZA, (c) P-20ZA, and (d) P-30ZA Coating on 304 Stainless Steel Substrate after Tape Test according to ASTM-D3359 Standard.

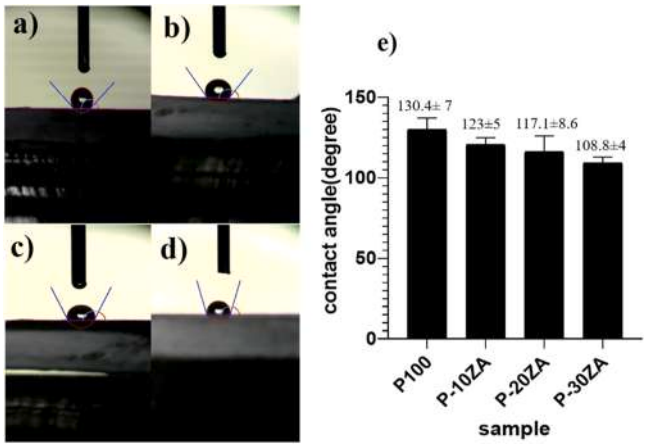

Fig. 14. Images of wettability measurement for (a) P100, (b) P-10ZA, (c) P-20ZA, (d) P-30ZA coating, and (e) diagram of contact angle changes of the coatings.

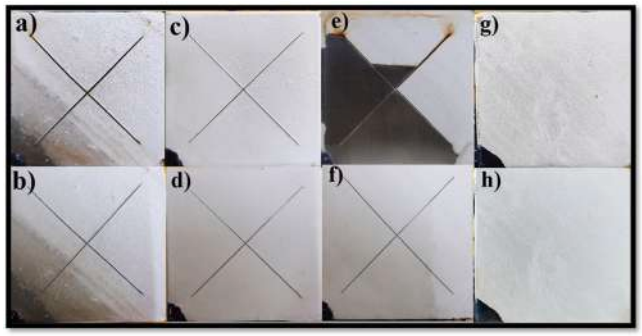

Fig. 15. Salt spray test (a,b) P-10ZA coating, (c,d) P-20ZA coating, (e,f) P-30ZA coating with scratches, (g,h) P-30ZA coating without scratches after 800 h of testing.

for 1000 h is equivalent to 15 years of exposure in a humid atmosphere; hence, a stabilizer-containing polyethylene coating can be effective under these conditions[38]. Zheng found that copper-containing polyethylene coatings (core, shell) produced by thermal spray in a seawater environment exhibit high corrosion resistance and anti-fouling properties due to the presence of copper as a biocide. He also deemed this polymeric coating highly suitable for marine applications[39].

In this study, considering the investigations that were conducted, it can be stated that polyethylene coatings contain 10 wt.% and 20 wt.% silver zeolite exhibits good adhesion with scratches. However, in the 30 wt.% silver zeolite sample, the adhesion of the coating has declined due to the reduced composite matrix and the accumulation of sodium ions in the environment beneath the coating, along with the formation of open-tail structures and NaOH products. Generally, organic coatings have voids, cavities, and defects in their structure, which can serve as pathways for the penetration of water molecules, ions, and oxygen. Due to their high specific surface area, adding silver zeolite particles to the polyethylene matrix results in a higher surface-to-volume ratio. It is also noteworthy that zeolite is highly hydrophilic. On the other hand, the boundary between the particle and the polymer is a susceptible area to water infiltration. Therefore, with its high surface area to volume ratio, the water-absorbent zeolite is more prone to water penetration, resulting in a more significant reduction in adhesion in the scratched sample P-30ZA due to increased water infiltration and accumulation. The P-30ZA sample exhibited a minor decrease in adhesion in the dry state, but a substantial reduction in coating adhesion was observed under the wet adhesion conditions due to water infiltration through the coating substrate interface. When water reaches the metal-coating joint season, three different mechanisms can be considered for adhesion loss. The first mechanism involves water accumulation in areas with lower adhesion strength, leading to localized and gradual expansion of reduced adhesion points under the coating. In the second mechanism, water reacts with the metal surface, causing corrosion and the formation of corrosion products. These materials often precipitate under the coating and at the joint season due to their poor solubility in the electrolyte. These materials are practically devoid of adhesion to the coating, resulting in the loss of adhesive bonds between the metal and the coating. The third mechanism involves the hydrolysis of the coating in the joint season and the partial destruction of the polymeric coating substrate connecting to the metal surface. In essence, the polymeric part of the boundary is degraded [40]. The 30 wt.% sample without scratches was exposed to the salt spray apparatus for 800 h, and no changes in adhesion and coating color were observed (g,h). It can be concluded that scratch-free samples exhibit durability beyond 800 h in a moist, saline environment.

3.9. Antibacterial

Fig. 16. illustrates samples P100, P-10ZA, P-20ZA, and P-30ZA for two bacterial culture environments, *E.coli.* (gram-negative), and *S. aureus* (gram-positive). In this test, the diameter of the wells considered for examination is 0.5 cm. For the control sample in both bacterial types, no halo formation occurred, and by adding silver zeolite, antimicrobial properties could be induced.

The 30 % silver zeolite sample formed the largest halo diameter (Fig. 16-h). Furthermore, the results indicate that the P-30ZA sample is more effective against gram-positive bacteria compared to gram-negative bacteria. This can be explained by the fact that gram-positive bacteria have a thick layer of peptidoglycan in their cell walls and lack an outer membrane. In contrast, gram-negative bacteria and a thin layer of peptidoglycan have a complex outer membrane made of lipopolysaccharide[41,42]. This outer membrane creates an additional protective layer, making them more resistant to antibiotics and immune responses and reducing bacterial permeability [38,43]. Based on the results of the antibiogram test using the halo diameter determination method, it can be stated that the P-30ZA sample exhibited the largest halo diameter against *E.coli.* and *S.aureus* bacteria, with values of 19.1 mm and 25.5 mm, respectively, compared to the 5 mm well

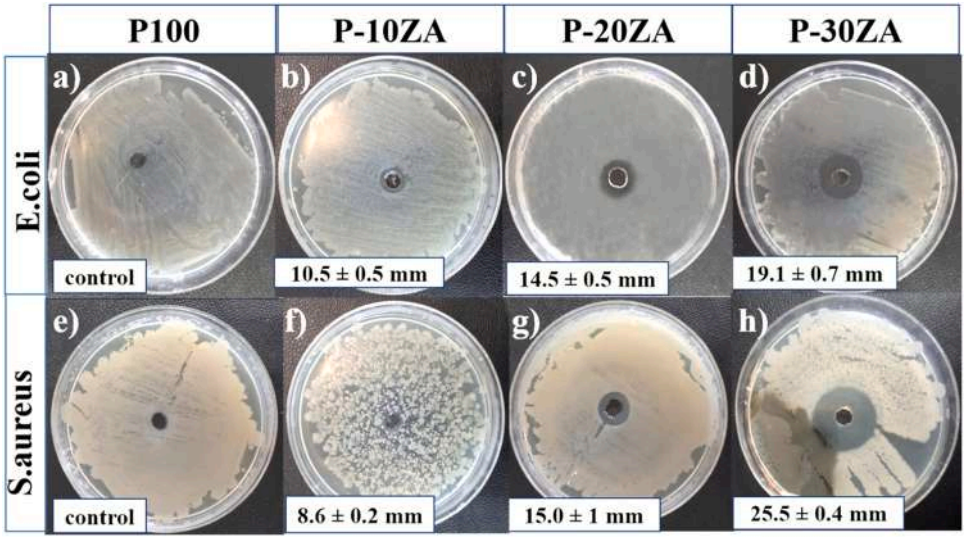

Fig. 16. Microbiological biogram test images using the no-growth ring determination method for P100, P-10ZA, P-20ZA, and P-30ZA samples in the culture medium of *E.coli.* (a, b, c, d) and *S.aureus* (e, f, g, h).

diameter. Therefore, this sample was selected and used for the colony count test. The sample was incubated for 24 h at 37 ± 2 °C with a density of 10^{-6} in the presence of bacteria in an agar-containing culture medium. It can be observed that the P-30ZA sample leads to a reduction in the bacterial count. This sample has the highest amount of silver incorporated into the clinoptilolite zeolite. In Fig. 17. it is evident that the colonies of *S.aureus* bacteria immediately after inoculation are 665, and after 24 h (c,d), this count has reduced to 114. the image related to the *E.coli.* bacterial colony is presented after being placed on the P-30ZA sample (a,b). In the left side of the image, it can be seen that at a temperature of 37 ± 2°C, the number of colonies immediately after inoculation was 205, but after 24 h, the count has reduced to 27. It can be inferred that the bacterial colony of *S. aureus* has exhibited a more pronounced response to silver ions compared to *E. coli*, leading to a greater reduction in the number of bacteria. As explained in the previous

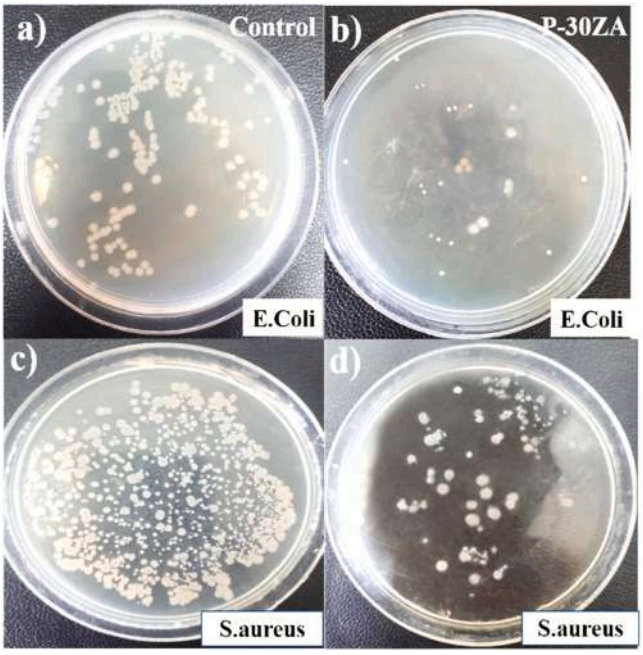

Fig. 17. Colonies counted in dilution 10^{-6} for sample P-30ZA in the culture medium of *E.coli* (a,b) and *S.aureus* bacteria (c,d).

section, considering that *S.aureus* bacteria have a thick layer of peptidoglycan and lack an outer membrane, silver ions demonstrate better permeability compared to *E. coli*. In addition to the peptidoglycan membrane, *E.coli* has a complex outer layer. In essence, the silver antimicrobial ion has a more significant impact on the genetics of *S. aureus* compared to *E.coli.*[28,44,45].

The antimicrobial evaluation of the silver-zeolite sample demonstrated a differential susceptibility among the tested microorganisms, with *Escherichia coli* (Gram-negative) exhibiting the highest sensitivity. The MIC for *E. coli* was observed at 3.9 mg/mL, with complete bactericidal effect (MBC) achieved at 7.81 mg/mL. In contrast, *Staphylococcus aureus* required slightly higher concentrations (MIC = 7.81 mg/mL, MBC = 7.81 mg/mL) for growth inhibition and bacterial eradication, while *Pseudomonas aeruginosa* showed increased resilience (MIC = 7.81 mg/mL, MBC = 15.62 mg/mL). The fungal strain *Aspergillus flavus* displayed markedly higher tolerance, requiring MIC and MFC values of 62.5 mg/mL and 250 mg/mL, respectively (Table 5).

The rapid inhibition of *Escherichia coli* can be attributed to its relatively thin peptidoglycan layer and higher outer membrane permeability, which facilitate efficient penetration of Ag^{+} ions. Once inside, these ions interact with critical cellular components, including thiol-containing enzymes, proteins, and nucleic acids, disrupting metabolic pathways, compromising membrane integrity, and ultimately inducing cell death. In comparison, *Staphylococcus aureus*, a Gram-positive bacterium with a thicker peptidoglycan wall, presents a more robust physical barrier, necessitating higher silver-zeolite concentrations to achieve comparable bactericidal effects[46,47]. Similarly, *Pseudomonas aeruginosa* exhibits intrinsic resistance mechanisms, such as efflux pumps and biofilm formation, which impede silver ion uptake and delay cell death. The antifungal activity observed against *Aspergillus flavus* further highlights the influence of structural and physiological barriers in microbial resistance; its rigid cell wall, composed of chitin and β-glucans, limits silver ion penetration, requiring elevated

Table 5
Comparison of the antimicrobial activities of silver zeolite.

microorganism	Silver zeolite	
	MIC (mg/mL)	MBC (mg/mL)
Escherichia coli	3.9	7.81
Staphylococcus aureus	7.81	7.81
Pseudomonas aeruginosa	7.81	15.62
Aspergillus flavus	62.5	250

concentrations for both growth inhibition and fungicidal activity. Overall, these findings demonstrate that silver-zeolite possess broad-spectrum antimicrobial efficacy, acting against Gram-negative bacteria (*E. coli* and *P. aeruginosa*), Gram-positive bacteria (*S. aureus*), and fungi (*A. flavus*). Notably, the coatings exhibit superior activity against *E. coli*, reflecting the greater susceptibility of Gram-negative strains due to their cell wall structure[48]. The controlled release of Ag^{+} ions from the zeolite matrix ensures sustained antimicrobial activity while minimizing cytotoxicity, indicating that silver-zeolite coatings can be tailored for rapid inhibition of more sensitive strains and adjusted for resilient pathogens. Silver-zeolite coatings demonstrated broad-spectrum antimicrobial efficacy against *Escherichia coli*, *Staphylococcus aureus*, *Pseudomonas aeruginosa*, and *Aspergillus flavus*, with notably higher activity against *E. coli* due to its thinner peptidoglycan layer and greater membrane permeability, enabling rapid Ag^{+} ion penetration[49,50]. Controlled ion release from the zeolite matrix ensures sustained antimicrobial performance across all tested microorganisms (Fig. 18).

4. Conclusion

In this research, natural clinoptilolite zeolite was washed with ethanol and hydrochloric acid. It then underwent ion exchange with silver nitrate in a temperature-controlled bath. Following this process, polyethylene composite coatings incorporating 0, 10, 20, and 30 wt% silver-loaded zeolite were applied to 304 stainless steel using the dip-coating method.

1. The calcium carbonate content in the natural clinoptilolite zeolite was significantly reduced through an acid-leaching process with hydrochloric acid. Silver-exchanged zeolite was then obtained by exchanging an ion with a 1:3 ratio of silver nitrate to zeolite for 16 h at 60°C.
2. A polyethylene coating was applied to silver-loaded zeolite using the dip-coating method, resulting in homogeneous, dense coatings over 100 microns in thickness. Infrared spectroscopy confirmed the presence of bonds associated with both polyethylene and zeolite. The optimal concentration of silver-loaded zeolite in the composite coating was up to 20 wt%, which enhanced the coating's adhesion. However, when the amount exceeded this concentration, the adhesion of the coating decreased.
3. The addition of silver-loaded zeolite to the high-density polyethylene matrix decreased the contact angle while remaining within the hydrophobic contact angle range. The surface roughness of the coating increased as the content of the ceramic composite material, silver-loaded zeolite, was raised.
4. The salt spray test results confirmed that the coating had high corrosion resistance; however, the P-30ZA scratched sample showed reduced adhesion due to the presence of blisters beneath the coating.
5. In the growth inhibition halo and colony count tests, increasing the silver-loaded zeolite content demonstrated improved antimicrobial properties against *S. aureus* compared to *E.coli*.
6. Silver-zeolite coatings showed broad-spectrum antimicrobial activity against *E. coli*, *S. aureus*, *P. aeruginosa*, and *A. flavus*, with MIC and MBC values indicating highest efficacy against *E. coli* due to its thinner peptidoglycan layer and greater membrane permeability.

CRediT authorship contribution statement

Soudabeh Shirani: Writing – original draft, Visualization, Software, Investigation, Formal analysis, Data curation. **EmadI Rahmatollah:** Writing – original draft, Supervision, Resources, Project administration, Funding acquisition, Formal analysis, Conceptualization. **Abdolmajid Eslami:** Writing – review & editing, Validation, Supervision, Resources, Project administration, Methodology. **Abdollah Saboori:** Writing – review & editing, Validation, Resources.

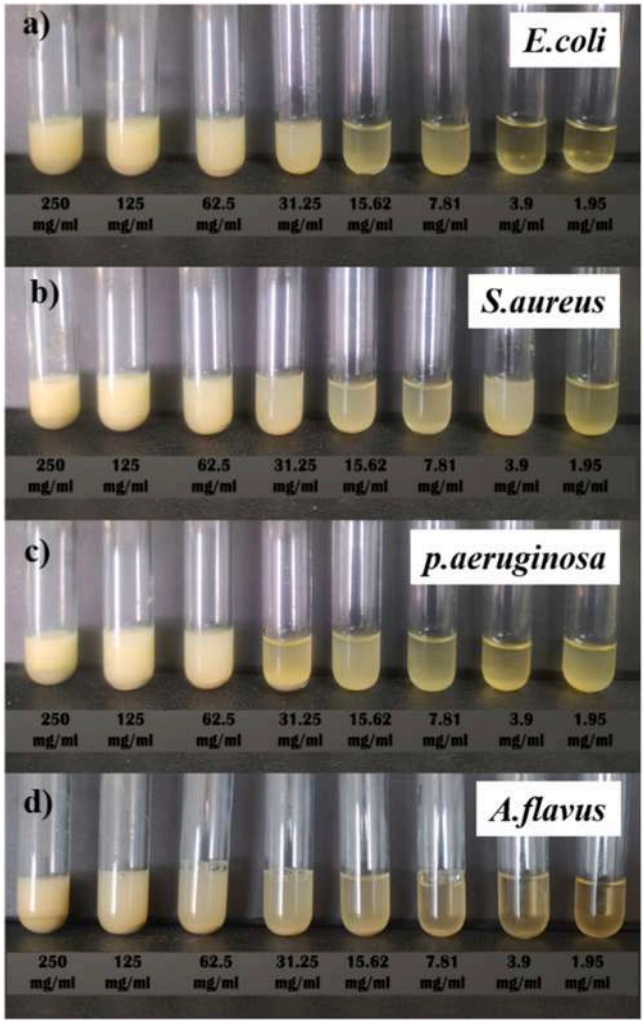

Fig. 18. Dilution series prepared from silver zeolite sample were tested against a)*E.coli* b)*S.aureus* c)*P.aeruginosa* bacteria strains, d)*A. flavus* fungal strain.

Declaration of Competing Interest

The authors declare that they have no known competing financial interests or personal relationships that could have appeared to influence the work reported in this paper.

Data availability

Data will be made available on request.

References

[1] J. Cui, R. Yeasmin, Y. Shao, H. Zhang, H. Zhang, J. Zhu, Fabrication of ag+, Cu2+, and Zn2+ ternary ion-exchanged zeolite as an antimicrobial agent in powder coating, Ind. Eng. Chem. Res. 59 (2) (2020) 751–762, https://doi.org/10.1021/acs.iecr.9b05338.
[2] J.R. Morones, et al., The bactericidal effect of silver nanoparticles, Nanotechnology 16 (10) (2005) 2346.
[3] A. Soleimani, F. Farahmandghavi, J. Morshedian, J. Keyvan Rad, Silver/hydrogen-exchanged zeolites embedded in modified polyethylene blends for antibacterial packaging with prolonged color stability, ACS Appl. Polym. Mater. 5 (4) (2023) 2917–2930, https://doi.org/10.1021/acsapm.3c00126.
[4] T. Wei, Y. Qu, Y. Zou, Y. Zhang, Q. Yu, Exploration of smart antibacterial coatings for practical applications, Curr. Opin. Chem. Eng. 34 (2021) 100727, https://doi.org/10.1016/j.coche.2021.100727.
[5] D.R. Monteiro, L.F. Gorup, A.S. Takamiya, A.C. Ruvollo-Filho, E.R. de Camargo, D. B. Barbosa, The growing importance of materials that prevent microbial adhesion: antimicrobial effect of medical devices containing silver, Int. J. Antimicrob. Agents 34 (2) (2009) 103–110, https://doi.org/10.1016/j.ijantimicag.2009.01.017.

[6] P. Dutta, B. Wang, Zeolite-supported silver as antimicrobial agents, Coord. Chem. Rev. 383 (2019) 1–29.
[7] N.K. Zeidan, N.M. Enany, G.G. Mohamed, E.S. Marzouk, The antibacterial effect of silver, zinc - oxide and combination of silver / zinc oxide nanoparticles coating of orthodontic brackets (an in vitro study), BMC Oral. Health (2022) 1–14, https://doi.org/10.1186/s12903-022-02263-6.
[8] T.T. Nguyen et al., "Silver — Gallium Nano-Amalgamated Particles as a Novel, Biocompatible Solution for Antibacterial Coatings," vol. 2310539, pp. 1–20, 2024, doi: 10.1002/adfm.202310539.
[9] N. Wattanawong, K. Chatchaipaiboon, N. Sreekirin, D. Aht-Ong, Migration, physical and antibacterial properties of silver zeolite/poly(butylene succinate) composite films for food packaging applications, J. Reinf. Plast. Compos 39 (3–4) (2020), https://doi.org/10.1177/0731684419893440.
[10] S. Abed, H.R. Bakhsheshi-Rad, H. Yaghoubi, L. Ning, A. Sadeghianmaryan, X. Chen, Antibacterial activities of zeolite/silver-graphene oxide nanocomposite in bone implants, Mater. Technol. 00 (00) (2020) 1–10, https://doi.org/10.1080/10667857.2020.1786784.
[11] C. Marambio-Jones, E.M.V. Hoek, A review of the antibacterial effects of silver nanomaterials and potential implications for human health and the environment, J. Nanopart. Res. 12 (5) (2010) 1531–1551, https://doi.org/10.1007/s11051-010-9900-y.
[12] L. Ferreira, J.F. Guedes, C. Almeida-Aguiar, A.M. Fonseca, I.C. Neves, Microbial growth inhibition caused by Zn/Ag-Y zeolite materials with different amounts of silver, Colloids Surf. B Biointerfaces 142 (2016) 141–147, https://doi.org/10.1016/j.colsurfb.2016.02.042.
[13] Z. Znak, et al., Improved modification of clinoptilolite with silver using ultrasonic radiation, Ultrason. Sonochem. 73 (2021) 105496, https://doi.org/10.1016/j.ultsonch.2021.105496.
[14] N. Mintcheva, M. Panayotova, G. Gicheva, O. Gemishev, G. Tyuliev, Effect of exchangeable ions in natural and modified zeolites on ag content, ag nanoparticle formation and their antibacterial activity, Materials 14 (15) (2021), https://doi.org/10.3390/ma14154153.
[15] V.E. Copcia, C. Luchian, S. Dunca, N. Bilba, C.M. Hristodor, Antibacterial activity of silver-modified natural clinoptilolite, J. Mater. Sci. 46 (22) (2011) 7121–7128, https://doi.org/10.1007/s10853-011-5635-0.
[16] H.R. Bakhsheshi-Rad, E. Hamzah, A.F. Ismail, M. Aziz, E. Karamian, N. Iqbal, Bioactivity, in-vitro corrosion behavior, and antibacterial activity of silver–zeolites doped hydroxyapatite coating on magnesium alloy, Trans. Nonferrous Met. Soc. China (Engl. Ed. 28 (8) (2018) 1553–1562, https://doi.org/10.1016/S1003-6326(18)64797-1.
[17] H. Serati-nouri, A. Jafari, L. Roshangar, M. Dadashpour, Materials science & engineering c biomedical applications of zeolite-based materials: a review, Mater. Sci. Eng. C. 116 (February) (2020) 111225, https://doi.org/10.1016/j.msec.2020.111225.
[18] S. Demirci, Z. Ustaoğlu, G.A. Yilmazer, F. Sahin, N. Baç, Antimicrobial properties of zeolite-X and zeolite-A ion-exchanged with silver, copper, and zinc against a broad range of microorganisms, Appl. Biochem. Biotechnol. 172 (3) (2014) 1652–1662, https://doi.org/10.1007/s12010-013-0647-7.
[19] P. Muangprakaew, N. Luangsa-Ard, J. Komasatitaya, Study of physical, mechanical, and barrier properties in linear Low-Density polyethylene mixed with silver zeolite nanoparticles (Ag-zeolite) film, Indian J. Sci. Technol. 14 (31) (2021) 2526–2534, https://doi.org/10.17485/ijst/v14i31.1.
[20] A.M. Pereyra, M.R. Gonzalez, T.A. Rodrigues, M.T. Soares Luterbach, E. I. Basaldella, Enhancement of biocorrosion resistance of epoxy coating by addition of Ag/Zn exchanged a zeolite, Surf. Coat. Technol. 270 (2015) 284–289, https://doi.org/10.1016/j.surfcoat.2015.02.044.
[21] W. He, et al., Enhanced anticorrosive, antimicrobial and biocompatible properties of AZ91D magnesium alloy by MAO-polycaprolactone-modified ZnO composite coating, Surf. Coat. Technol. 494 (2024) 131484, https://doi.org/10.1016/j.surfcoat.2024.131484.
[22] A. Trentin, A. Pakseresht, A. Duran, Y. Castro, D. Galusek, Electrochemical characterization of polymeric coatings for corrosion protection: a review of advances and perspectives, Polymers 14 (12) (2022) 1–28, https://doi.org/10.3390/polym14122306.
[23] A. Michalik, Conductive Polymers for Corrosion Protection: Acritical Investigation (Ph. D Thesis), Ruhr-Bochum-University, 2009.
[24] S.K. Singh, S.P. Tambe, G. Gunasekaran, V.S. Raja, D. Kumar, Electrochemical impedance study of thermally sprayable polyethylene coatings, Corros. Sci. 51 (3) (Mar. 2009) 595–601, https://doi.org/10.1016/j.corsci.2008.11.025.
[25] L. Li, G. Cheng, X. Chen, Zeolitic imidazolate frameworks dispersed in waterborne epoxy resin to improve the anticorrosion performance of the coatings, e-Polymers 22 (1) (2022) 883–897, https://doi.org/10.1515/epoly-2022-0079.
[26] S. Jeong, D. Kim, J. Seo, Preparation and antimicrobial properties of LDPE composite films melt-blended with polymerized urushiol powders (YPUOH) for packaging applications, Prog. Org. Coat. 85 (2015) 76–83, https://doi.org/10.1016/j.porgcoat.2015.03.012.
[27] Z. Jia, et al., Flame spray fabrication of polyethylene-Cu composite coatings with enwrapped structures: a new route for constructing antifouling layers, Surf. Coat. Technol. 309 (Jan. 2017) 872–879, https://doi.org/10.1016/j.surfcoat.2016.10.071.
[28] N. IQBAL, et al., Zinc-doped hydroxyapatite—zeolite/polycaprolactone composites coating on magnesium substrate for enhancing in-vitro corrosion and antibacterial performance, Trans. Nonferrous Met. Soc. China 30 (1) (2020) 123–133, https://doi.org/10.1016/S1003-6326(19)65185-X.
[29] M.M. Salim, N. Ahmad, N. Nik, Characterization and antibacterial activity of silver exchanged regenerated NaY zeolite from surfactant-modi fi ed NaY zeolite, Mater. Sci. Eng. C 59 (2016) 70–77, https://doi.org/10.1016/j.msec.2015.09.099.
[30] I. Tirouni, M. Sadeghi, M. Pakizeh, Separation of C3H8 and C2H6 from CH4 in polyurethane–zeolite 4Å and ZSM-5 mixed matrix membranes, Sep. Purif. Technol. 141 (Feb. 2015) 394–402, https://doi.org/10.1016/j.seppur.2014.12.012.
[31] X. Xu, H. Ding, B.K. Wang, Preparation and performance of Ag+-Zn2+-Zeolite antimicrobial and antibacterial plastic, Adv. Mater. Res. 96 (Jan. 2010) 151–154, https://doi.org/10.4028/www.scientific.net/AMR.96.151.
[32] M. Rivera-Garza, M.T. Olguın, I. Garcıa-Sosa, D. Alcántara, G. Rodrıguez-Fuentes, Silver supported on natural Mexican zeolite as an antibacterial material, Microporous Mesoporous Mater. 39 (3) (2000) 431–444.
[33] M. Abareshi, S.M. Shahroodi, 'EFFECT OF SILVER NANOPARTICLES ON THE CRYSTALLINITY BEHAVIOR OF POLYETHYLENE,' presented at the IRANIAN PHYSICAL CHEMISTRY CONFERENCE. 2013, [Online]. Available: ⟨https://sid.ir/paper/916238/en⟩."
[34] E. Matin, M.M. Attar, B. Ramezanzadeh, Investigation of corrosion protection properties of an epoxy nanocomposite loaded with polysiloxane surface modified nanosilica particles on the steel substrate, Prog. Org. Coat. (2014), https://doi.org/10.1016/j.porgcoat.2014.07.004.
[35] Z. Hayati, B. Hoomehr, F. Khalesi, K. Raeissi, Synthesis and electrophoretic deposition of TiO2-SiO2 composite nanoparticles on stainless steel substrate, J. Alloy. Compd. 931 (Jan. 2023) 167619, https://doi.org/10.1016/j.jallcom.2022.167619.
[36] A. Daneshnia, K. Raeissi, P. Salehikahrizsangi, Rapid one-step electrodeposition of robust superhydrophobic and oleophobic ni coating with anti-corrosion and self-cleaning properties, Surf. Coat. Technol. 450 (Nov. 2022) 129007, https://doi.org/10.1016/j.surfcoat.2022.129007.
[37] M.A. Golozar, R. Bagheri, Quality of high density polyethylene on plain carbon steel and the role of primers, ESTEGHLAL 19 (1) (2000) 23–34. ⟨https://sid.ir/paper/5889/en⟩ ([Online]. Available).
[38] M.A. Golozar, R. Bagheri, High-density polyethylene coating on carbon steel by an electrostatic powder spray system, J. Appl. Polym. Sci. 70 (12) (Dec. 1998) 2507–2513, doi: 10.1002/(SICI)1097-4628(19981219)70:12<2507::AID-APP24>3.0.CO;2-Y.
[39] Z. Jia, et al., Surface & coatings technology flame spray fabrication of polyethylene-Cu composite coatings with enwrapped structures: a new route for constructing antifouling layers, Surf. Coat. Technol. (2016), https://doi.org/10.1016/j.surfcoat.2016.10.071.
[40] J. Bachert, A.H.M.E. Rahman, M. Abu-Ayyad, Anti-corrosive coating using recycled high density polyethylene for automotive chassis, ASME Int. Mech. Eng. Congr. Expo. Proc. 12 (2018) 1–9, https://doi.org/10.1115/IMECE2018-86498.
[41] E.L. Pavlova, E.P. Nenova, L.D. Yocheva, I.A. Ivanova, P.A. Georgiev, Antimicrobial and oxidative activities of different levels of Silver-Exchanged zeolites x and ZSM-5 and their ecotoxicity, Pharmaceuticals 17 (12) (Nov. 2024), https://doi.org/10.3390/ph17121586.
[42] F. Russo, B. Furlan, M. Calovi, O. Massidda, S. Rossi, Silver-based vitreous enamel coatings: assessment of their antimicrobial activity towards escherichia coli and staphylococcus aureus before and after surface degradation, Surf. Coat. Technol. 445 (2022) 128702, https://doi.org/10.1016/j.surfcoat.2022.128702.
[43] W. Pongnop, K. Sombatsompop, A. Kositchaiyong, N. Sombatsompop, Effects of incorporating technique and silver colloid content on antibacterial performance for thermoplastic films, J. Appl. Polym. Sci. 122 (5) (Dec. 2011) 3456–3465, https://doi.org/10.1002/app.34448.
[44] Q.L. Feng, J. Wu, G.Q. Chen, F.Z. Cui, T.N. Kim, J.O. Kim, A mechanistic study of the antibacterial effect of silver ions on escherichia coli and staphylococcus aureus, J. Biomed. Mater. Res. 52 (4) (2000) 662–668.
[45] L. Tosheva, S. Belkhair, M. Gackowski, S. Malic, N. Al-Shanti, J. Verran, Rapid screening of the antimicrobial efficacy of ag zeolites, Colloids Surf. B Biointerfaces 157 (2017) 254–260, https://doi.org/10.1016/j.colsurfb.2017.06.001.
[46] L.A. Suleiman, R. Haddadin, H.A. Hodali, Pages 61-68 antimicrobial activity of Metal-Loaded zeolites against 'S. aureus' and 'E. coli', Jjc 14 (2) (2019) 61–68.
[47] S. Panda, S. Rath, M. Garhanayak, S.C. Bidyasagar Bal, R. Nagarajappa, In vitro evaluation of antimicrobial efficacy of silver zeolite against common oral pathogens, Rocz. Panstw. Zakl. Hig. / Ann. Natl. Inst. Hyg. 72 (2) (2021) 203–208, https://doi.org/10.32394/rpzh.2021.0161.
[48] S. Egger, R.P. Lehmann, M.J. Height, M.J. Loessner, M. Schuppler, Antimicrobial properties of a novel silver-silica nanocomposite material, Appl. Environ. Microbiol 75 (9) (2009) 2973–2976, https://doi.org/10.1128/AEM.01658-08.
[49] G.D. Savi, et al., New ion-exchanged zeolite derivatives: antifungal and antimycotoxin properties against aspergillus flavus and aflatoxin B1, Mater. Res. Express 4 (8) (2017) 0–9, https://doi.org/10.1088/2053-1591/aa84a5.
[50] S. Chen, J. Popovich, N. Iannuzo, S.E. Haydel, D.K. Seo, Silver-ion-exchanged nanostructured zeolite x as antibacterial agent with superior ion release kinetics and efficacy against methicillin-resistant staphylococcus aureus, ACS Appl. Mater. Interfaces 9 (45) (2017) 39271–39282, https://doi.org/10.1021/acsami.7b15001.